Energy Engineering

Tech Science Press

DOI: 10.32604/ee.2023.041410

ARTICLE

The Influence of Acid on the Rock Mechanical Characteristics of Deep Shale in the Wujiaping Formation

Hao Zhang[1], Yan Zhang[1,*], Wei Liu[2], Ximin Zhang[3] and Xiang Liu[2]

[1]School of Petroleum Engineering, Yangtze University, Wuhan, 430100, China

[2]Petroleum Engineering Technology Research Institute, Jianghan Oilfield Branch of Sinopec, Wuhan, 430035, China

[3]Drilling Technology Research Institute, Sinopec Shengli Oilfield Service Corporation, Deyang, 618000, China

[*]Corresponding Author: Yan Zhang. Email: yanzhang@yangtzeu.edu.cn

Received: 21 April 2023 Accepted: 29 June 2023 Published: 27 December 2023

ABSTRACT

The microscopic characteristics and mechanical properties of rocks change after the action of acid on deep shale, which affects the fracturing effect. Accordingly, we designed and conducted indoor experiments related to the changes in macro and microscopic characteristics after the interaction of acid with the shale of Wujiaping Formation, based on which the characteristic law of fracture volume modification after acid fracturing was studied using numerical simulation. The results demonstrate that the pores and fractures are enlarged and the structure is significantly loosened after the acid immersion. And a 15% concentration of hydrochloric acid can effectively dissolve shale. Furthermore, the degree of acid-etching reaction is highly variable because of the different carbonate content, which reveals the strong inhomogeneity of the shale system in the Wujiaping Group reservoir section. After the acid interacted with the shale rock samples, the triaxial compressive strength, elastic modulus, and Poisson's ratio of shale decreased. Moreover, the evaluation of the effect after acid fracturing simulated by fracturing software revealed that the smaller the value of elastic modulus in shale-based reservoirs, the more favorable the fracture volume modification. This discovery not only provides a theoretical basis for the expansion and extension patterns of acid-fracturing in carbonaceous shale formations but also offers research methods and theoretical insights for the fundamental exploration of other deep-seated oil and gas resources.

KEYWORDS

Shale; acid fracturing; macro characteristics; microscopic characteristics; mechanical properties

Nomenclature

q	The total pumped fluid volume
V_l	The fluid loss volume
V_{sp}	The initial fluid loss volume
p	The fluid momentum
DFN	The discrete fracture network
x_w, y_w, z_w	The borehole location and perforation locations of the DFN grid centre
x_{Dw}, y_{Dw}, z_{Dw}	The borehole location and perforation locations of the given grid centre
b	The maximum extension distance of fracture in Y-Z plane
λ	The aspect ratio of increasing production volume

a	The length of the main fracture in the X direction
L_{DFN}	The total length of fracture network
A_{DFN}	The total area of fracture network
V_{DFN}	The total volume of fracture network
L_ζ	The total length of fracture network in the direction of "ζ"
A_ζ	The total area of fracture network in the direction of "ζ"
V_ζ	The total volume of fracture network in the direction of "ζ"
V_{SR}	The stimulation reservior volume of fracture network
$\overline{h}$	The average reconstruction height after volume fracturing
γ_E	The stiffness coefficient of each plane
ϕ_E	The stiffness factor
ψ_E	The equivalent strength coefficient
E_ζ	The equivalent strength
E	Elastic modulus
μ	Poisson's ratio

1 Introduction

The Permian shale formation system in China has good prospects for shale gas exploration [1] and is currently in the initial exploration and development stage. The Permian Wujiaping Formation is a set of interbedded limestone and mud shale developed in the eastern Sichuan-western Hubei area. The shales of the Wujiaping Formation are horizontally laminated, with carbonaceous filling between single-layer shale joints and microfractures filled with calcite [2]. Acid fracturing is a proven measure to increase oil and gas production in these reservoirs. Given that acid and other fluids entering the formation will deteriorate the strength of rocks, change the microscopic characteristics of reservoir pores and fractures, and affect the mechanical properties of shale reservoirs, it is necessary to study the laws affecting the macroscopic mechanical and microscopic characteristics of shale after acid enters the formation.

Studies focusing on the laws of acid influence on the mechanical properties of carbonate rocks have been reported both at home and abroad. Some scholars have studied the effect of acid on the macroscopic mechanical properties of rock. Li et al. confirmed that chemical corrosion has a significant softening effect on tuffs, but the degree of softening is not enough to change the brittle damage mode [3]. Alameedy et al. studied the changes in mechanical characteristics of carbonate rocks after acid treatment and found that the dynamic Young's modulus decreases, while the Poisson's ratio, the coefficient of lateral earth pressure at rest, and the material index all increase [4]. Teklu et al. found that the use of dilute acid before, after, or during hydraulic fracturing of carbonate-rich shale reservoirs changed the reservoir's pore-permeability structure, softening the strength of the rock and increasing production [5]. Wu et al. confirmed the effect of acid on pore connectivity after fracturing in carbonate-rich mineral shales, i.e., both porosity and permeability increased after acid injection [6,7]. Du et al. provided the potential laws of pore size and the elastic modulus evolution of shale in the process of point-source acid erosion [8].

Other scholars have studied the influence of acid on the microscopic characteristics of rock. Berner found that the rock acid erosion pattern was controlled by two types of erosion, surface reaction, and solute diffusion, during the acid contact reaction; the corresponding microscopic acid erosion characteristics under different conditions could be identified [9]. Chen et al. conducted a study on the microstructural changes of limestone after acidification using acoustic velocity tests

and electron microscope scanning. They found that the pore distribution in limestone exhibits fractal characteristics, and the fractal dimension does not exhibit a linear relationship with soaking time [10]. Miao et al. used scanning electron microscopy (SEM) and electron spectroscopy to observe and analyze the effects of acid corrosion on the microstructure, defect morphology, and mineral elements of granite [11]. Sheng et al. established a direct correlation between the dissolution effect and the microfracturing mechanisms [12]. Xu et al. conducted acid dissolution experiments on dolomite with different microstructures and found that dolomite with a loose microstructure had a faster acid reaction, a rougher etched surface, but lower embedding strength compared to dolomite with a compact microstructure [13]. Chen et al. used 5% HCl or 15% H_2O_2 reactive fluids to evaluate the generation of micro-sized pores and microfractures in Longmaxi shale and their potential for mitigating water blockage [14]. Zhang et al. investigated the impact of clean acid and gelled acid on carbonate formations. The results revealed that gelled acid reduced compressive strength and Poisson's ratio, while clean acid reduced tensile strength and Young's modulus. Clean acid led to a smaller and narrower acid-affected area, whereas gelled acid resulted in a larger and broader etched region. The study concluded that channel etching and a higher calcite content were conducive to higher fracture conductivity [15].

The current research lacks multiple perspectives to analyse the macro- and fine-scale characteristic patterns of the shale-based formation after interaction with acid [16–19]. In this paper, using the acid system used in the field, we carry out a study of the acid action on the deep shale of the Wujiaping Formation in the Lichuan area and conduct a multi-angle analysis from the change in microscopic pore-fracture characteristics to macroscopic mechanical characteristics. On this basis, the effect of different elastic parameters on fracturing fractures after acid action was studied, which not only provides a strong theoretical basis for acid fracturing in Wujiaping Formation shale but also provides a research method and practical reference for the efficient development of deep shale.

2 Microscopic Characteristics of Shale after Acid Action

2.1 Experimental Rock Samples

The experimental rock samples were taken from the subsurface of the Permian Wujiaping Formation in the Hongxing Block of Lichuan at about 3,300 m. The samples were drilled along the shale laminae surface. We analysed mineral fractions of the shales of the Wujiaping Formation using X-ray diffraction (XRD) analysis. The test results demonstrated that the total clay minerals in the rock samples of this formation were distributed from 15% to 38%, the quartz was distributed from 21% to 49%, the carbonate was distributed from 25% to 31%, and the pyrite was distributed from 4% to 12%-indicating that the carbonate rock content of Wujiaping Formation is high.

2.2 Analysis of Microscopic Characteristics

Hydrochloric acid (HCl) is the most common acid employed to lower the shale rock strength during hydraulic fracturing. We carried out acid etching experiments with different concentrations of hydrochloric acid and rock samples. The experimental results showed that 15% HCl can significantly dissolve the rock samples, which is shown in Fig. 1. In order to study the microscopic damage characteristics of Wujiaping shale after soaking in acid solution, three rock samples S1, S2, and S3 with different initial structures were selected (due to the different mineral content).

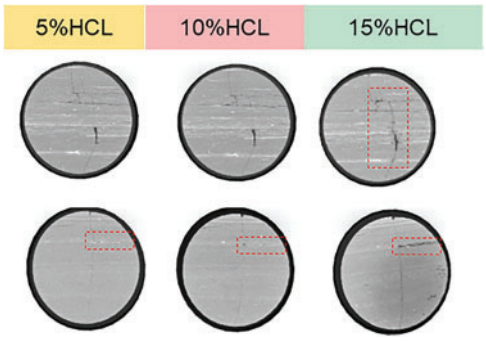

Figure 1: Results of different concentrations of hydrochloric acid etching shale

Microstructures (such as microfractures) inside the rocks were observed and studied before and after acid immersion (initially, after 2 h of 15% HCl immersion) using a Hitachi SU8010-Hitachi environmental scanning electron microscope. The expansion and evolution characteristics after the acid entered the pores and microfractures of the shale were analysed, as depicted in Figs. 2–4.

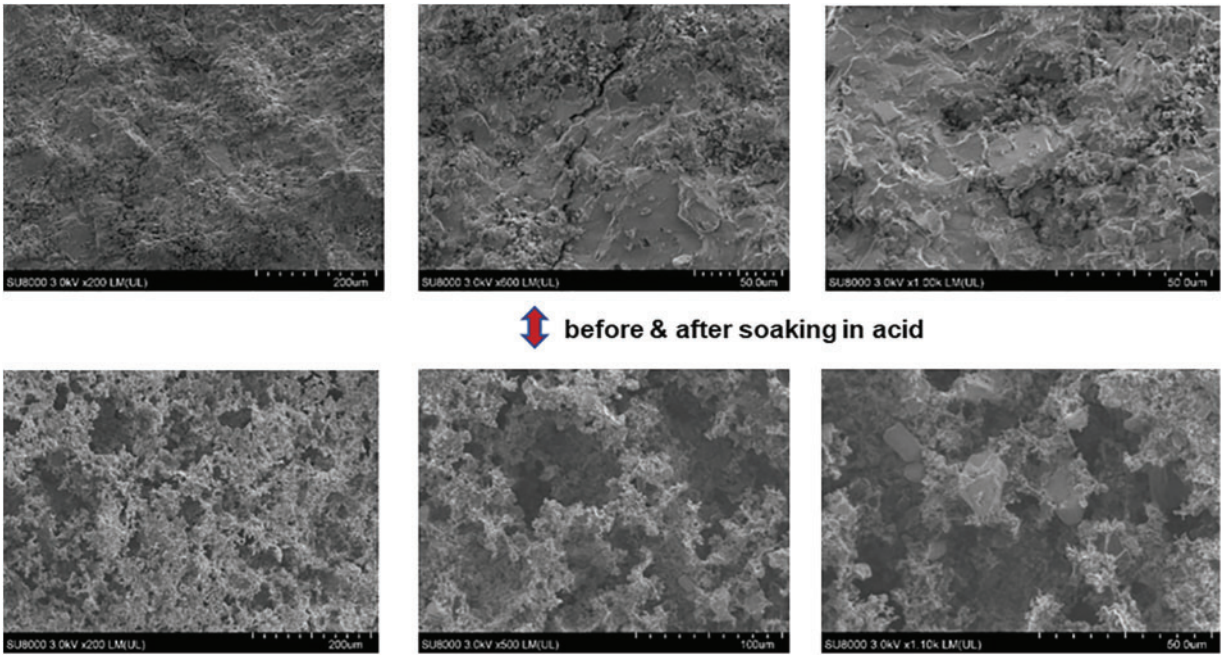

Figure 2: Comparison of sample S1 collected from Wujiaping before and after soaking in 15% HCl

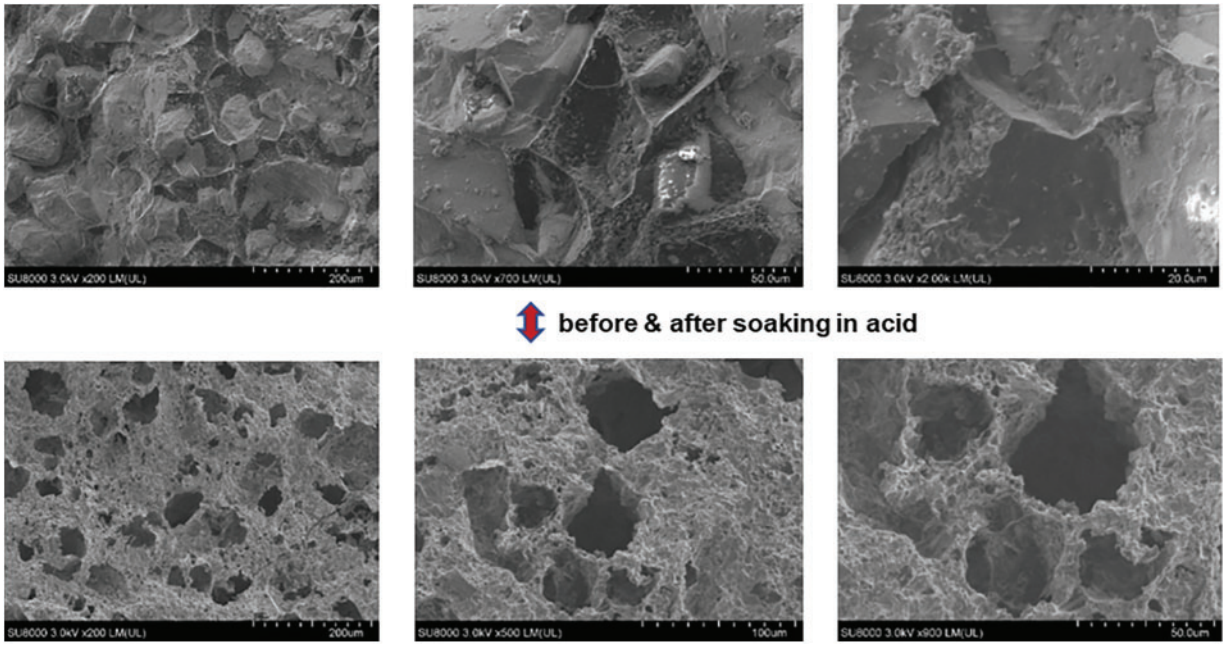

Figure 3: Comparison of sample S2 collected from Wujiaping before and after soaking in 15% HCl

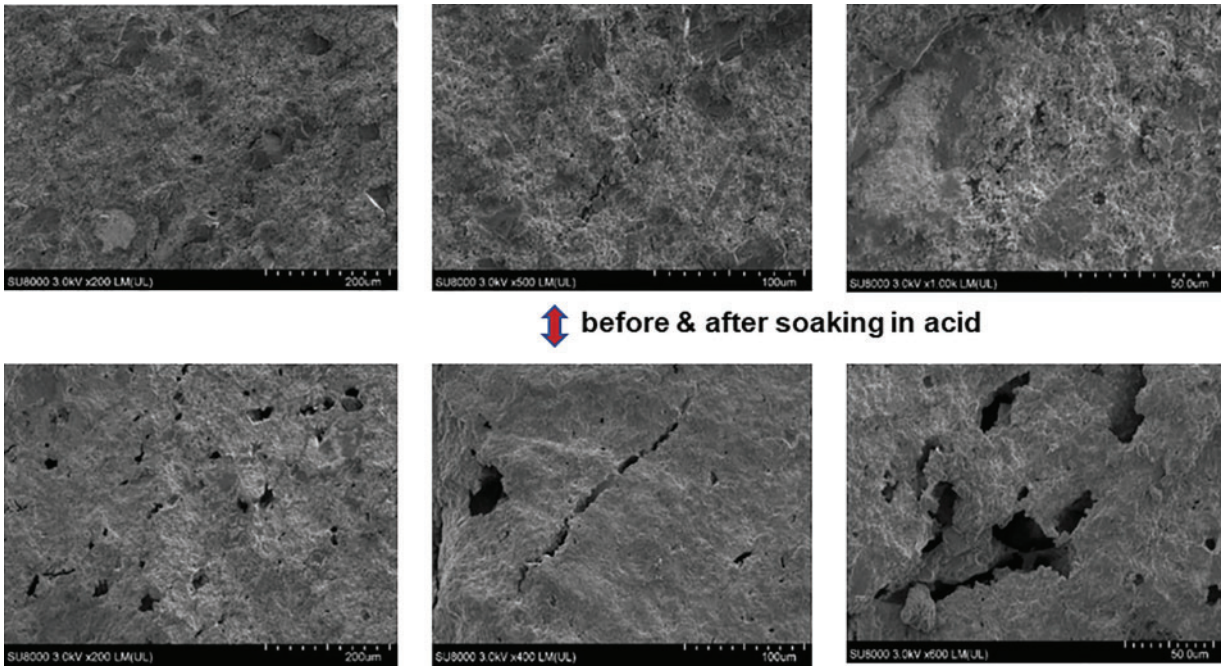

Figure 4: Comparison of sample S3 collected from Wujiaping before and after soaking in 15% HCl

In general, after soaking in 15% HCl, the pores and fractures of the rock samples are obviously larger. The S1 sample has evident microfractures initially, and the structure is loose after acid soaking. The S2 sample has a denser structure initially, and after acid rot soaking, there are more connected

pores. The S3 sample initially has microfractures with a loose structure and several pores, and after acid soaking, there are still microfractures but more unconnected pores. The main action site of the acid is found to be the feldspar and calcite-filled area, which is depicted in Fig. 5. The main reactions are presented by Eqs. (1) and (2), as shown below:

$$CaCO_3 + 2HCL \rightarrow CaCL_2 + H_2O + CO_2 \uparrow \quad (1)$$

$$CaMg(CO_3)_2 + 4HCL \rightarrow CaCL_2 + MgCL_2 + 2H_2O + 2CO_2 \uparrow \quad (2)$$

Besides, the changes of pore volume and porosity of rock samples before and after acid treatment were tested, and the results showed that the pore volume and porosity increased after hydrochloric acid treatment. This is depicted in Fig. 6.

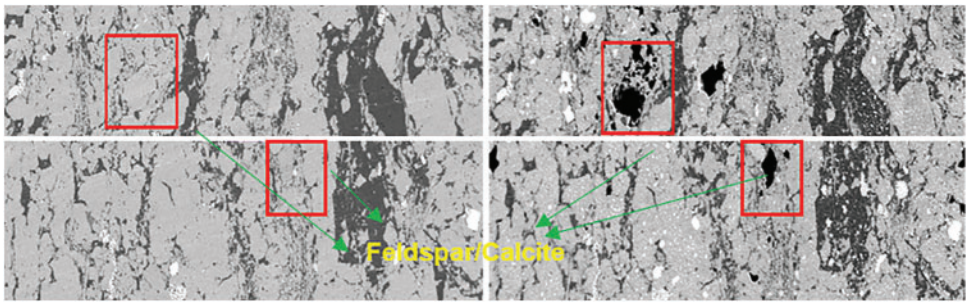

Figure 5: The main action site of the acid

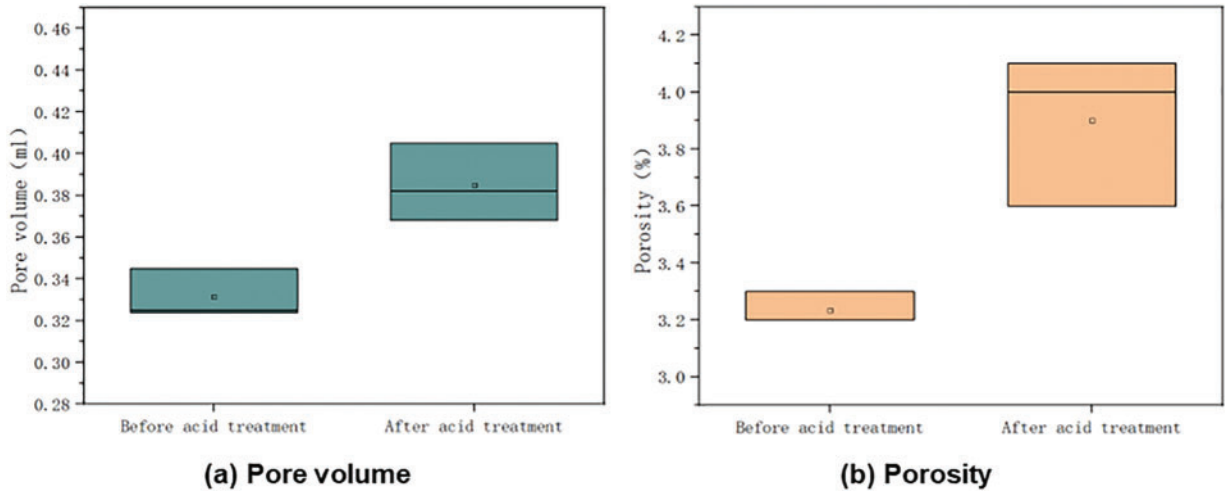

Figure 6: Pore volume and porosity of rock samples before and after acid treatment

3 Mechanical Properties of Shale after Acid Action

The rock's mechanical properties characterise its deformation and damage during external disturbance and the influence of the acid, which is directly related to the law of fracture expansion and the post-fracture effect after the acid action. This section explores the macroscopic effects of acid on the mechanical properties of shale.

3.1 Experimental Method

The shale of the Wujiaping Formation was soaked in 15% HCl for 2 h under normal temperature and pressure so that the core was completely immersed in acid to produce a full interaction. Then, the mechanical properties of the rock were tested using a TAW2000 rock triaxial testing machine, and the compressive strength, elastic modulus, and Poisson's ratio of the rock were measured.

3.2 Analysis of Mechanical Properties of Shale

Four samples were drilled in the same full-size core in the same direction at two different depths of 3,305.81 and 3,294.83 m respectively for comparison experiments to analyse the effect of acid on shale, numbered X1, X2 and Y1, Y2. The obtained experimental data are presented in Table 1. The failure mode of rock samples after the triaxial compressive strength test is depicted in Fig. 7. The damage of untreated samples under triaxial stress conditions in Wujiaping Formation shale is predominantly splitting and shear damage. The brittleness of the rock is weakened after increasing the surrounding pressure, and the fracture expansion after rock damage does not connect. The damage of rocks under triaxial stress conditions of Wujiaping Formation shale after acid soaking is affected by acid erosion, and the rock extension laminae joints expand and illustrate horizontal joints. Shear damage is nonetheless formed by triaxial stress, with a communication phenomenon among the fractures.

Table 1: Mechanical parameters of shale before and after acid immersion

Depth (m)	Number	Soaking time (h)	Length before soaking (mm)	Length after soaking (mm)	Diameter before soaking (mm)	Diameter after soaking (mm)	Modulus of elasticity (GPa)	Poisson's ratio	Compressive strength (MPa)	Surrounding pressure (MPa)
3,305.81	X1	0	51.18	/	24.72	/	60.64	0.32	323.78	20
	X2	2	50.90	50.86	24.34	24.34	54.04	0.24	303.80	
3,294.83	Y1	0	51.88	/	24.72	/	45.03	0.26	257.82	
	Y2	2	50.72	50.08	24.52	24.52	7.89	0.20	60.48	

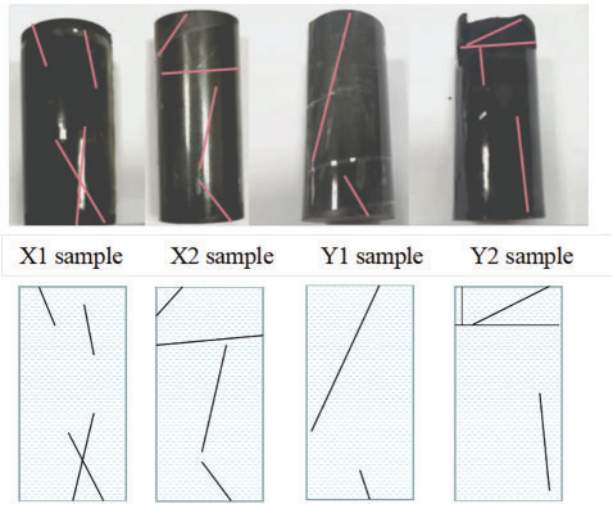

Figure 7: Three-axis strength destruction form of treated and untreated samples in Wujiaping

From the reaction between acid and core, the core of 3,294.83 m well depth reacts violently with hydrochloric acid, and the core length decreased by 0.64 mm after soaking for 2 h, while the length of 3,305.81 m shale core does not change much, which is related to the higher carbonate content of Y rock sample than that of X rock sample.

From the obtained rock mechanical parameters, the compressive strength, elastic modulus, and Poisson's ratio of shale collected from Wujiaping Formation decreased after soaking in 15% HCl for 2 h. The decrease of core compressive strength and elastic modulus of 3,294.83 m well depth is much larger than that of 3,305.81 m, while Poisson's ratio reduction was negligible.

4 Effect of Shale Hydraulic Fracture Morphology

Based on the rule that the compressive strength, elastic modulus, and Poisson's ratio of rock decrease after acid fracturing in deep shale, fracturing analysis software was used to further analyse the fracturing effect of acid fracturing in deep carbonate-bearing shale formation by simulating the law of reservoir fracture propagation and extension caused by the change in rock mechanical parameters after acid fracturing.

In this study, based on the theory of discontinuous medium, through the discrete fracture network model, the fracture morphology of fracture and pore dual-porosity medium was used to simulate the characteristics of multiple fractures, cluster–complex–cluster, and discrete fracture network formed by shale gas in unconventional oil and gas reservoirs. Seven assumptions were made to simplify the model:

1) The main crack expands perpendicular to the minimum principal stress $\sigma 3$ direction in the X-Z plane, perpendicular to $\sigma 2$ in the Y-Z plane, and perpendicular to $\sigma 1$ in the X-Y plane.

2) The discrete fracture network consists of three planes of secondary cracks in the X-Z, Y-Z, and X-Y planes, and the gap spacings are Δy, Δx, and Δz.

3) When the pressure in the fracture is greater than the minimum horizontal principal stress in the corresponding plane, the fracture extends only in Y-Z and X-Z planes.

4) The fractures are elliptical.

5) Inter-slit interference effects are considered.

6) The effects of fluid lag and expansion at the fracture tip are ignored.

7) The hydraulic fracture extends only to a specific limit in the plane.

As depicted in Fig. 8, the volume of fluid flowing into the fracture should equal the volume of the total pump fluid minus the fluid loss volume and then minus the initial fluid loss volume. Therefore, the state equation of the natural fracture fracturing model is:

$$\int_0^t q\,(t)\,dt - V_l\,(t) - V_{sp}\,(t) = V_f\,(t) \tag{3}$$

After combining the momentum equation of the fluid:

$$\frac{dp}{dx} = -\frac{f}{2}\frac{\rho\,(\overline{v})^2}{d_h} = -\frac{f}{2}\frac{\rho q^2}{\pi^3 a^2 b^3} \tag{4}$$

The primary characteristic parameters of the discrete fracture network (DFN) model include the number of the fracture network, the total length of the fracture network, the area of the fracture network, the amount of liquid loss, and the volume of the fracture network. In a given mesh module,

the positions of borehole and perforation are determined by dimensionless coordinates (x_{DW}, y_{DW}, z_{DW}):

$$x_{DW} = \frac{2x_w}{\Delta x}, y_{DW} = \frac{2y_w}{\Delta y}, z_{DW} = \frac{2z_w}{\Delta z} \tag{5}$$

where x_w, y_w, and z_w are the borehole location and perforation locations of the DFN grid centre.

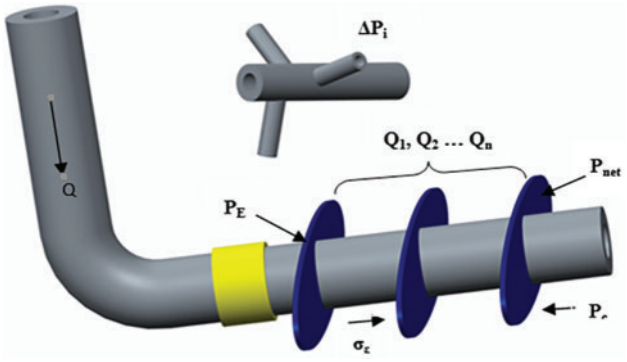

Figure 8: Flow and pressure distribution diagram of shale staged fracturing

The maximum extension range of fractures in the Y-Z plane (short axis) is:

$$b = \lambda a \tag{6}$$

where "λ" is the aspect ratio of increasing production volume, and "a" is the length of the main fracture in the X direction.

The total length, area, and volume of the fracture network [20] are:

$$L_{DFN} = \sum_{\zeta=x,y,z} \left\{ \sum_{j=1}^{N_\zeta} L_\zeta(j) \right\}$$

$$A_{DFN} = \sum_{\zeta=x,y,z} \left\{ \sum_{j=1}^{N_\zeta} A_\zeta(j) \right\}$$

$$V_{DFN} = \sum_{\zeta=x,y,z} \left\{ \sum_{j=1}^{N_\zeta} V_\zeta(j) \right\} \tag{7}$$

where "ζ" is the maximum extension length of the fracture network in the direction of "ζ".

$$L_\zeta = \int d\zeta$$

$$A_\zeta = \int h_\zeta(\zeta)\, d\zeta$$

$$V_\zeta = \int \omega_\zeta(\zeta)\, h_\zeta(\zeta)\, d\zeta$$

$$\overline{\omega_\zeta} = \frac{V_\zeta}{A_\zeta} \tag{8}$$

Stimulation reservoir volume of the fracture network is:

$$V_{SR} = \int_A h(\zeta)\, d\zeta = \pi ab\bar{h} \tag{9}$$

where "$\bar{h}$" is the average reconstruction height after volume fracturing, and "πab" is the ellipsoid area of fracture network fracturing. The crack length in the X direction (main fracture) is "a", and the fracture extension length in the Y direction is "b".

When the fracture distance is close, each fracture will be affected by the stress field of adjacent fractures, and inter-fracture interference occurs. The stiffness coefficient of each plane is defined as:

$$\gamma_E = (N_\zeta - 1)\,\phi_E \tag{10}$$

where "ϕ_E" is the stiffness factor, which is related to fracture spacing and fracture geometry, and "N_ζ" is the number of parallel fractures. If $\phi_E = 0$, there is no inter-fracture interference between fractures, and the stiffness coefficient γ_E is 0. If $\phi_E = 1$, there is complete interference between fractures.

At this time, the stiffness coefficient $(\gamma_E)_{\max}$ is "$N_\zeta - 1$", and generally $\gamma_E \leq (\gamma_E)_{\max}$. Because of inter-fracture interference, each fracture is squeezed by the adjacent fracture. The width and length of the fracture are limited, and the net pressure in the fracture increases. Therefore, this interference is equivalent to the increase in the strength of the rock mass itself, and the equivalent strength coefficient is defined as ψ_E:

$$\psi_E = \gamma_E + 1 \tag{11}$$

The equivalent strength E_ζ is:

$$E_\zeta = \psi_E E \tag{12}$$

where "E" is the elastic modulus of the rock mass.

The numerical model stratigraphic parameter inputs are based on the basic physical and mechanical parameters of shale in the study area obtained from indoor tests. Based on relevant research results [21–23], the physical and mechanical parameters of the matrix body and laminae of the simulated shale strata are initially determined as presented in Table 2.

Table 2: Physical and mechanical parameters of Wujiaping Formation shale reservoir

Parameters	Value
Burial depth (m)	3,300
Porosity (%)	5.0
Permeability (mD)	0.001
Pore pressure gradient (MPa/100 m)	1.04
Elastic modulus (GPa)	25.03–60.64
Poisson's ratio	0.2–0.32
Compressive strength (MPa)	250–320

The development of critical shale gas reservoir technology requires using the volume fracturing process to ensure the formation of complex network fractures. This paper focuses on the effect of rock elastic parameters on fracture extension and expansion. Based on the fracturing model, the fracture extension states are simulated at the elastic moduli of 57.55, 47.55, 37.55, and 27.55 GPa.

For elastic moduli of 57.55, 47.55, 37.55, and 27.55 GPa, the total lengths of the fracture network are 5,308.6, 5,483.3, 5,557.0 and 6,026.5 m, and the lengths of generated secondary fractures are 4,877.6, 5,045.3, 5,116.0 and 5,568.5 m. This is shown in Fig. 9. According to the simulation results, (1) the total fracture length in the discrete fracture network model gradually increases as the elastic modulus decreases; (2) the total length of secondary fractures formed by fracturing accounts for 92% of the total fracture length, indicating that secondary fractures contribute the majority of the drainage area.

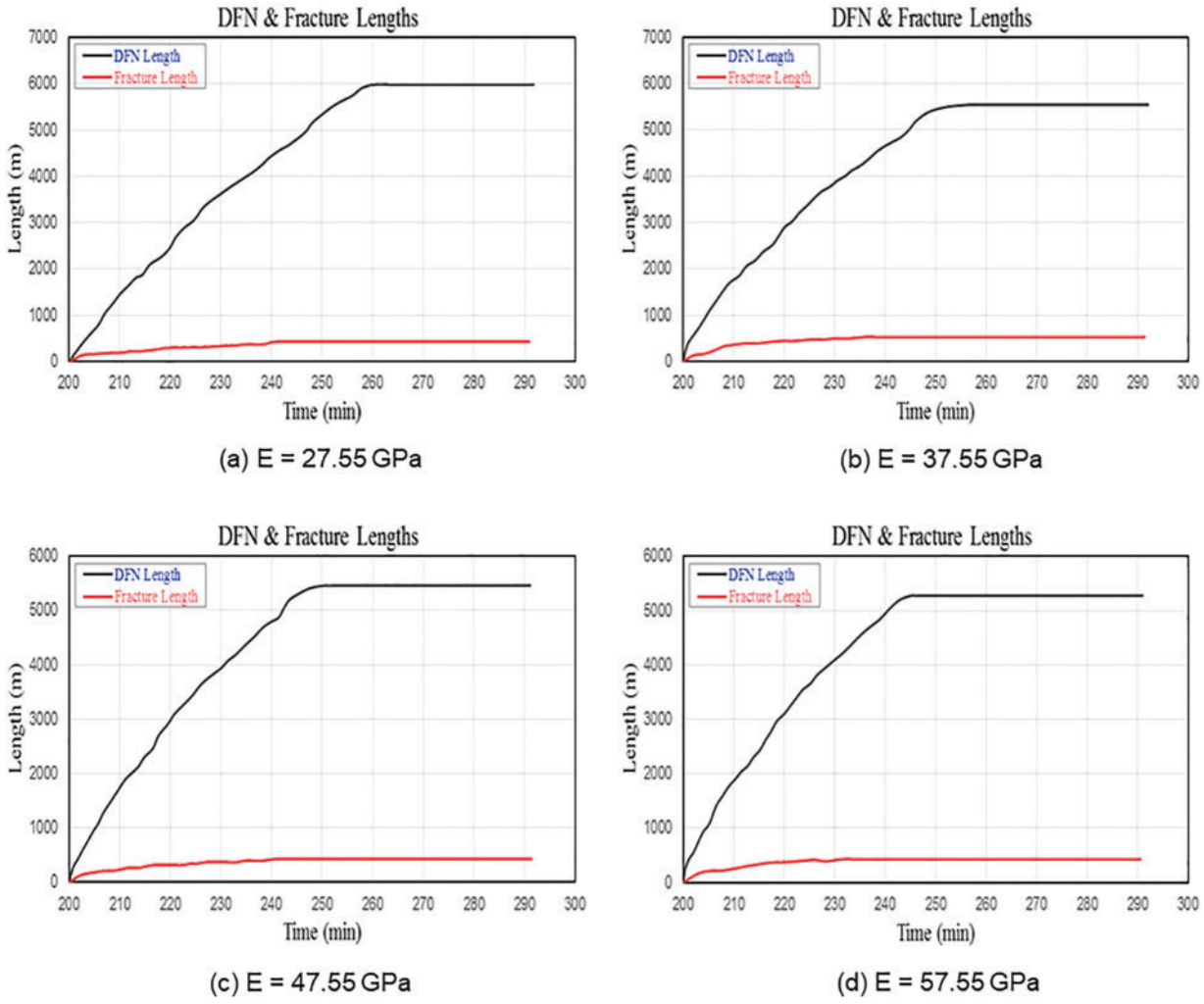

Figure 9: Total lengths of DFN and fracture under different elastic moduli

As depicted in Fig. 10, for elastic moduli of 57.55, 47.55, 37.55, and 27.55 GPa, the reservoir reconstruction volumes are 2.8477 × 106 m^3, 2.8906 × 106 m^3, 2.8921 × 106 m^3 and 2.9513 × 106 m^3. According to the simulation results, it is found that the reservoir modification volume tends to increase gradually as the elastic modulus decreases.

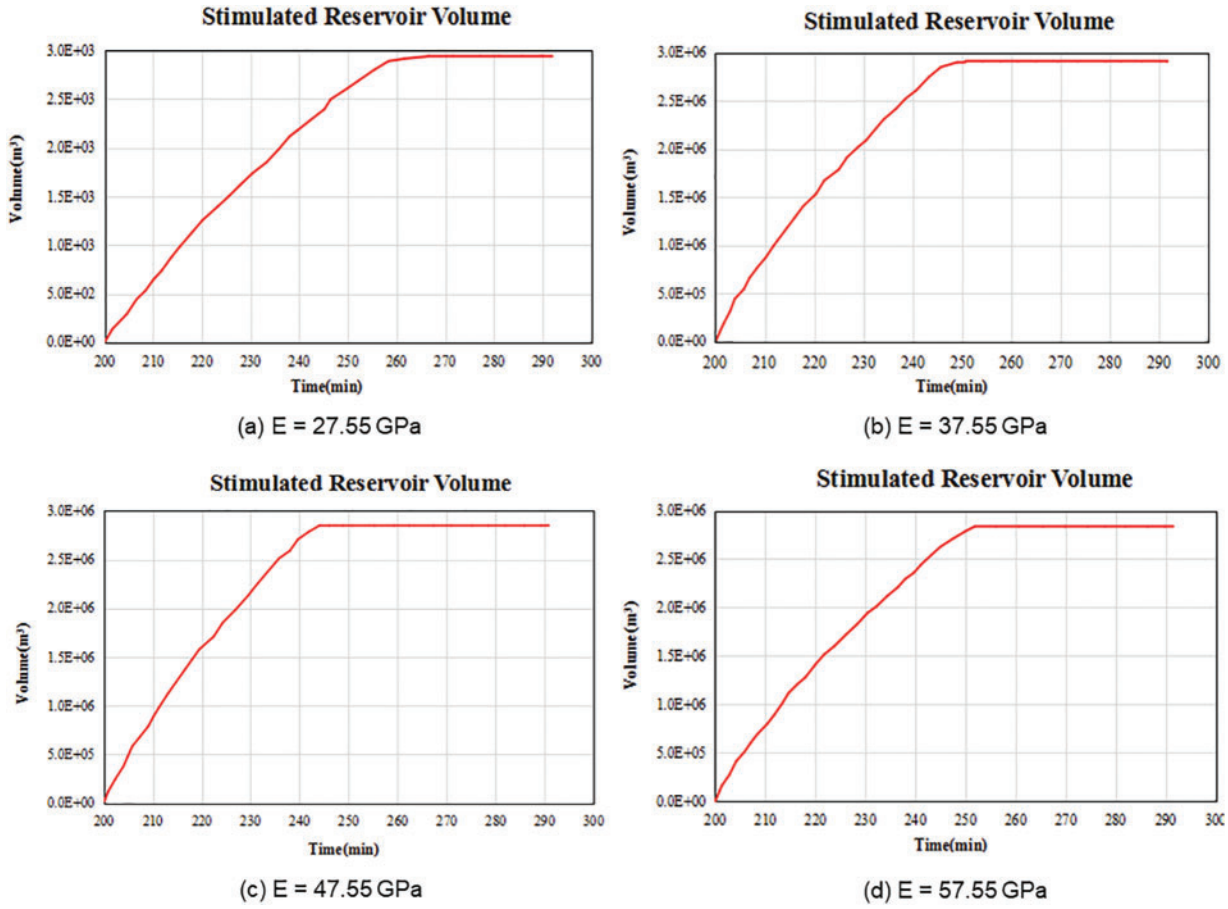

Figure 10: Reservoir reconstruction volume under different elastic moduli

As depicted in Fig. 11, for elastic moduli of 57.55, 47.55, 37.55, and 27.55 GPa, the average fracture width of the fracture network are 0.1753, 0.1767, 0.1807 and 0.1852 cm, and the average fracture width of the generated secondary fracture are 0.1728, 0.1743, 0.1782 and 0.1827 cm. According to the simulation results, it is found that (1) the average seam width in the discrete fracture network model and the average seam width of the secondary fractures formed by fracturing gradually increases as the elastic modulus decreases; (2) the average seam width of the secondary fractures is significantly lower than that of the dominant fractures, indicating that the dominant fractures contribute the main fracture conductivity.

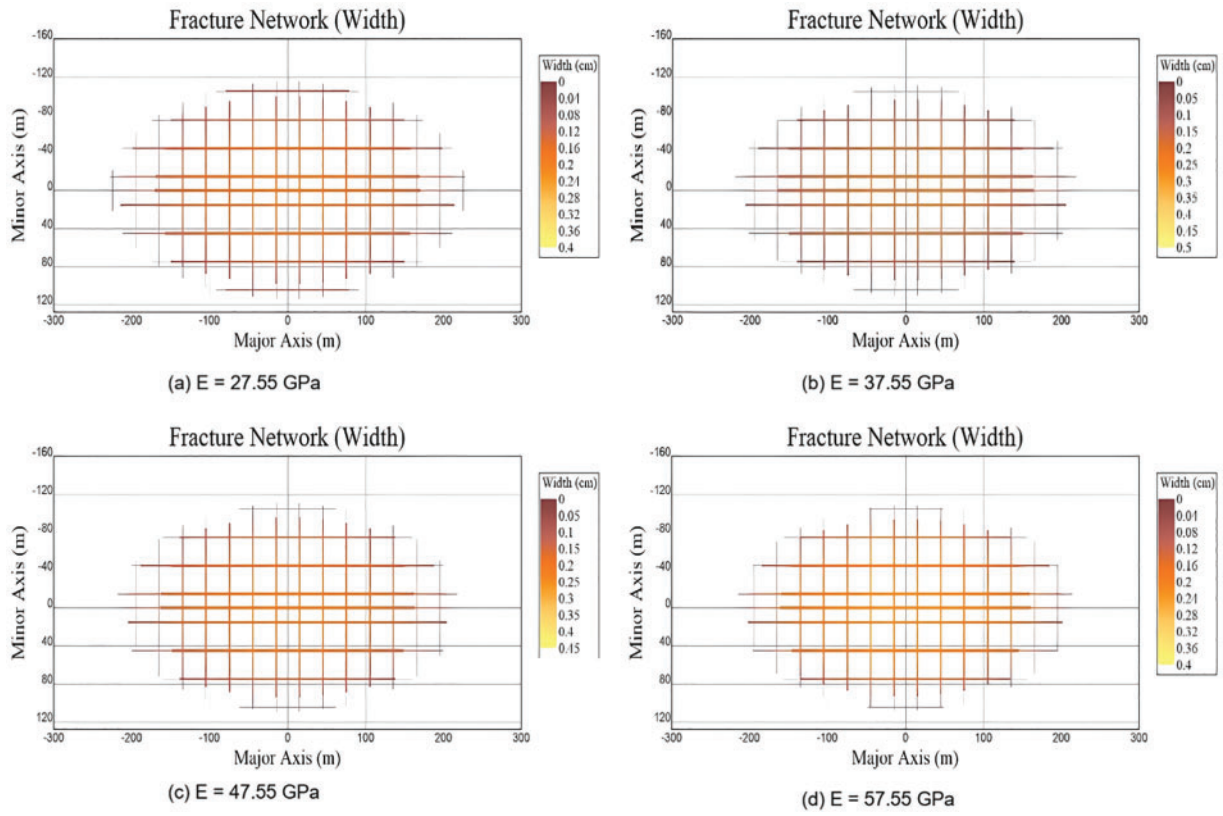

Figure 11: Average width of fracture network under different elastic moduli

5 Results and Discussion

Based on the simulation results, the elastic modulus has a significant effect on the extension and elongation of the fracture. The larger the elastic modulus, the fracture length, fracture width and reformed volume of the reservoir are more restricted, indicating that this parameter has a stronger negative impact on the artificial fracture. In this study, for every 1 GPa decrease in elastic modulus, the total seam length increased by 22.274 m and the average seam width increased by 0.0003 cm. This is depicted in Fig. 12.

Generally speaking, rock with higher Young's modulus has a stronger ability to resist deformation under the action of stress, resulting in the fractures in the rock with higher Young's modulus having a larger flow space under the action of effective stress, and therefore a larger permeability. However, rocks with higher Young's modulus usually have fewer fractures and lower permeability. Zhou et al. [24] proposed that microfractures are the main factor in increasing the permeability of shale. The reaction of carbonate minerals with acid will produce more microfractures, which can effectively increase the permeability of shale. However, it is worth discussing that the acid will reduce the elastic modulus of the rock and increase the fracture length and width as well as the volume of reservoir modification, while it also tends to close the microfractures with the increase of effective stress, leading to the decrease of permeability. Therefore, when considering acid fracturing, a suitable proppant should be considered to ensure that the fracture can be effectively supported.

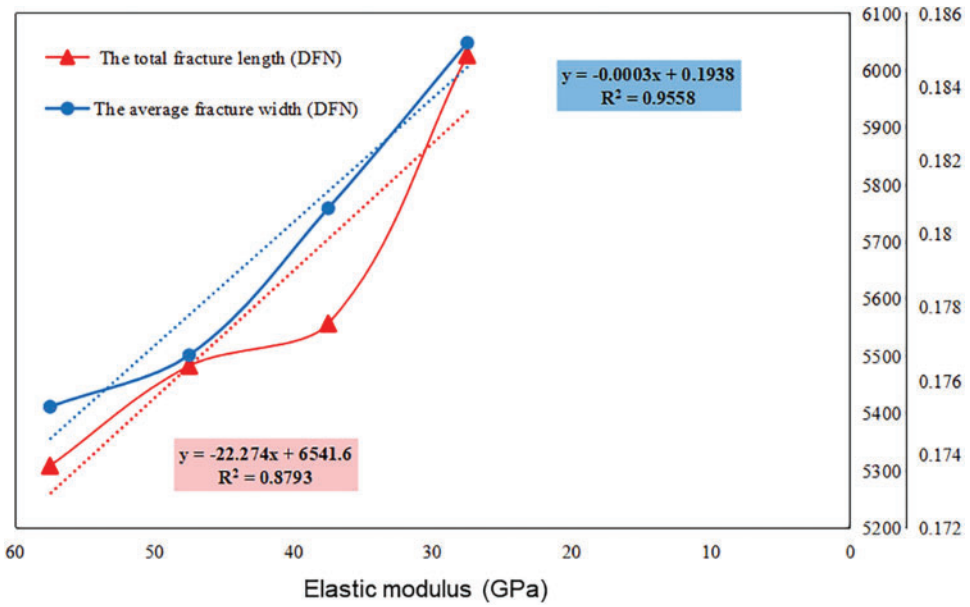

Figure 12: Relationship between total length & average width of fracture network and elastic moduli

6 Conclusion

1. The pores and fractures of Wujiaping Formation shale increased after the action of the acid solution, and the structure was loose after acid soaking. Some samples produced more connected pores after the action of the acid solution, whereas some produced more unconnected pores. This phenomenon is related to carbonate content, and action mechanism, revealing strong heterogeneity of the shale series in the Wujiaping Formation.

2. The triaxial compressive strength, elastic modulus, and Poisson's ratio of shale decrease after the interaction of acid and shale samples. The total fracture length, average fracture width, and reservoir modification volume of fracture formation gradually increase with the decrease of elastic modulus. Secondary fractures contribute to the vast majority of oil discharge areas, and the average fracture width of secondary fractures is significantly lower than that of dominant fractures, indicating that the dominant fractures contribute to the primary fracture conductivity.

Acknowledgement: Thank you for the information provided by Sinopec.

Funding Statement: This study is supported by a Scientific Research Project of Sinopec (Program No. P21087-2), the Open Fund of Key Laboratory of Marine Oil & Gas Reservoirs Production, Sinopec (Grant No. 33550000-22-FW2099-0004).

Author Contributions: The authors confirm contribution to the paper as follows: study conception and design: Yan Zhang and Hao Zhang; data collection: Wei Liu and Xiang Liu; analysis and interpretation of results: Yan Zhang, Hao Zhang and Ximin Zhang; draft manuscript preparation: Hao Zhang. All authors reviewed the results and approved the final version of the manuscript.

Availability of Data and Materials: The data presented in this study are available on request from the corresponding author.

Conflicts of Interest: The authors declare that they have no conflicts of interest to report regarding the present study.

References

1. Zou, C. N., Dong, D. Z., Wang, S. J., Li, J. Z., Li, X. J. et al. (2010). Geological characteristics, formation mechanism and resource potential of shale gas in China. *Petroleum Exploration & Development, 37(6),* 641–653.
2. Zhao, P. P., Gao, B., Guo, Z. F., Wei, Z. H. (2020). Exploration potential of marine-continental transitional and deep-water shelf shale gas in the Upper Permian, Sichuan Basin. *Petroleum Geology & Experiment, 42(3),* 335–344 (In Chinese).
3. Li, H., Zhong, Z. L., Liu, X. R., Sheng, Y., Yang, D. M. (2018). Micro-damage evolution and macro-mechanical property degradation of limestone due to chemical effects. *International Journal of Rock Mechanics and Mining Sciences, 110,* 257–265.
4. Alameedy, U., Alhaleem, A. A., Isah, A., Al-Yaseri, A., Mahmoud, M. et al. (2022). Effect of acid treatment on the geomechanical properties of rocks: An experimental investigation in Ahdeb oil field. *Journal of Petroleum Exploration and Production Technology, 12(12),* 3425–3441.
5. Teklu, T., Amini, K., Park, D., Jung, H., Abass, H. et al. (2017). Effect of dilute acid on hydraulic fracturing of carbonate rich shales–Modeling study. *SPE Eastern Regional Meeting*, SPE-187533-MS. Kentucky, USA.
6. Wu, W. W., Russell, R., Sharma, M. (2020). Non-uniform etching-the key for an effective acid fracturing in shale: An experimental study. *Unconventional Resources Technology Conference*, pp. 1340–1362. Texas, USA.
7. Khalil, R. E., Emadi, H., Gamadi, T. (2020). An experimental investigation analyzing effects of injection pressure on efficiency of matrix acidizing stimulation on Marcellus shale core samples. *ARMA US Rock Mechanics/Geomechanics Symposium*, ARMA-2020-1294. Colorado, USA.
8. Du, S. H. (2021). Potential laws on the changes of shale in acid erosion process based on the fast matching method of dimensional analysis. *International Journal of Hydrogen Energy, 46(11),* 7836–7847.
9. Berner, R. A. (1978). Rate control of mineral dissolution under earth surface condition. *American Journal of Science, 278(9),* 1235–1252.
10. Chen, X. M., Liu, X. P., Luo, H. M., Long, L. J., Liu, C. J. (2022). Microscopic damage to limestone under acidic conditions: Phenomena and mechanisms. *Sustainability, 14(18),* 11771.
11. Miao, S. J., Cai, M. F., Guo, Q. F., Wang, P. T., Liang, M. C. (2016). Damage effects and mechanisms in granite treated with acidic chemical solutions. *International Journal of Rock Mechanics and Mining Sciences, 88,* 77–86.
12. Sheng, M., Khan, W. A., Cheng, S. Z., Zhang, P. P., Tian, S. C. et al. (2021). Characteristics of micro-fracturing in shales induced by dilute acid. *Journal of Natural Gas Science and Engineering, 88,* 103855.
13. Xu, P., Sheng, M., Lin, T. Y., Liu, Q., Wang, X. G. et al. (2022). Influences of rock microstructure on acid dissolution at a dolomite surface. *Geothermics, 100,* 102324.
14. Chen, Q., Hu, H. P., Kang, Y. L., You, L. J., Zhou, Y. et al. (2022). Mitigating water blockage in shale matrix by acidizing or oxidizing treatment: Evidence from transport pathway change and diffusivity enhancement. *Journal of Petroleum Science and Engineering, 219,* 111132.
15. Zhang, R. X., Hou, B., Zhou, B. C., Liu, Y. J., Xiao, Y. et al. (2020). Effect of acid fracturing on carbonate formation in Southwest China based on experimental investigations. *Journal of Natural Gas Science and Engineering, 73,* 103057.
16. Morsy, S., Sheng, J. J., Soliman, M. Y. (2013). Improving hydraulic fracturing of shale formations by acidizing. *SPE Eastern Regional Meeting*, SPE-165688-MS. Pennsylvania, USA.

17. Cash, R., Zhu, D., Hill, A. D. (2016). Acid fracturing carbonate-rich shale: A feasibility investigation of eagle ford formation. *SPE Asia Pacific Hydraulic Fracturing Conference*, SPE-181805-MS. Beijing, China.
18. Jiang, T. X., Bian, X. B., Wang, H. T., Li, S. M. (2017). Volume fracturing of deep shale gas horizontal wells. *Natural Gas Industry, 37(1),* 90–96.
19. Veytskin, Y. B., Tammina, V. K., Bobko, C. P., Hartley, P. G., Clennell, M. B. et al. (2017). Micromechanical characterization of shales through nanoindentation and energy dispersive X-ray spectrometry. *Geomechanics for Energy and the Environment, 9,* 21–35.
20. Bruce, R. M., Lucas, W. B. (2011). A discrete fracture network model for hydraulically induced fractures - theory, parametric and case studies. *SPE Hydraulic Fracturing Technology Conference and Exhibition*, SPE-140514-MS. Texas, USA.
21. Song, T., Li, S. Z., Zhang, Y. L., Bao, H. Y., Liu, H. T. et al. (2023). Gas differential enrichment characteristics and controlling factors of Upper Permian marine shale in western Hubei area: A case study of Wujiaping formation II in Hongxing block and Dalong formation in Enshi area. *Natural Gas Geoscience, 34(8),* 1425–1441 (In Chinese).
22. Liu, Q. (2023). Logging evaluation of gas–bearing potential in wujiaping formation shale gas reservoir in Hongxing area. *Journal of Jianghan Petroleum University of Staff and Workers, 36(2),* 35–38 (In Chinese).
23. Tang, L. J., Guo, T. L., Jin, W. Z., Yu, Y. X., Li, R. F. (2008). Main structural styles and deformation mechanisms in the Northern Sichuan Basin, Southern China. *Acta Geologica Sinica, 82(3),* 543–553.
24. Zhou, Z., Abass, H., Li, X. P., Teklu, T. (2016). Experimental investigation of the effect of imbibition on shale permeability during hydraulic fracturing. *Journal of Natural Gas Science and Engineering, 29,* 413–430.